Supplementary Information for "Chiral Magnon Dynamics in a Kitaev Magnet Revealed by Magneto-Optics"

Kartik Panda[1†], Chaebin Kim[2†], Daniel Bazyliansky[1†], Javier Taboada-Gutiérrez[3], Florian Le Mardelé[4], Jan Dzian[4,5], Guy Levy[1], Jae Ha Kim[6], Youjin Lee[7], Bumchan Park[8], Martin Mourigal[2], Jae Hoon Kim[8], Alexey B. Kuzmenko[3], Milan Orlita[4], Je-Geun Park[7*], Nimrod Bachar[1*]

[1]Department of Physics, Ariel University, Ariel, 4070000, Israel.
[2]School of Physics, Georgia Institute of Technology, Atlanta, 30332, Georgia USA.
[3]Department of Quantum Matter Physics, Université de Genève, 24 Quai Ernest Ansermet, Geneva, CH-1211, Switzerland.
[4]LNCMI-EMFL, CNRS UPR3228, Université Grenoble Alpes, Université Toulouse, Université Toulouse 3, INSA-T, Grenoble and Toulouse, France.
[5]Institute of Physics, Charles University, Ke Karlovu 5, Prague, 121 16, Czech Republic.
[6]Center for Nano Materials, Sogang University, Seoul, 04107, Republic of Korea.
[7]Department of Physics and Astronomy, Seoul National University, Seoul, 08826, Republic of Korea.
[8]Department of Physics, Yonsei University, Seoul, 03722, Republic of Korea.

*Corresponding author(s). E-mail(s): jgpark10@snu.ac.kr; nimib@ariel.ac.il;
†These authors contributed equally to this work.

A. Evolution of magnon excitations with field and easy axis model

Figure S1(a) presents the evolution of the square of the relative central frequency, $\Delta\omega = \omega(B) - \omega(0)$, of the two magnons as a function of the square of the applied magnetic field up to 16 T. The first electromagnon mode, centered around 34 cm^{-1}, shows a relatively modest blue shift, with its frequency increasing by approximately 2.5% over the applied field range. In contrast, the second electromagnon mode, centered near 37 cm^{-1}, exhibits a more pronounced shift of about 7% as the magnetic field increases to 16 T. Initial attempts to model the field dependence of the magnon modes using an easy-axis model, $\omega(B)^2 = \omega_0^2 + g\mu_B B^2$, did not accurately capture the observed frequency shifts across the full range of magnetic fields. In an easy-axis model [1, 2], $\Delta\omega^2$ should be linear in B^2, which is not valid in our case, as can be seen in Figure S1(a).

B. Spectral weight of Circular Dichroism

The field dependence of the circular dichroism can also be seen through the spectral weight of the peaks in $\Im\{\sigma_{xy}\}$. We have integrated the area below each peak in $\Im\{\sigma_{xy}\}$ and show the result of the spectral weight:

$$W_{xy} \propto \int_{\omega_1}^{\omega_2} \Im\{\sigma_{xy}(\omega)\}\, d\omega. \tag{1}$$

as a function of the increasing magnetic field up to 7 T. Here we have considered $\omega_1 = 32.34$ cm^{-1} and $\omega_2 = 35.06$ cm^{-1} for the first peak and $\omega_1 = 35.06$ cm^{-1} and $\omega_2 = 38.8$ cm^{-1}for the second peak. Figure S1(b) shows the spectral weight W_{xy} of two excitations as a function of magnetic field, where we have taken the absolute value for the area of the lower excitation. The increasing magnetic field shifts the peak position slightly, as was already observed in the transmission spectra, but also for the linear increase of W_{xy} as a function of magnetic field.

C. THz Magnetic circular dichroism

Figure S1(c)-(f) presents the peak positions of circularly polarized absorption spectra of the lower (34 cm^{-1}) and upper (37 cm^{-1}) magnon modes in NiI_2. Panels (c) and (d) display the magnetic field evolution of the absorption peaks for the lower mode under LCP and RCP excitation, respectively. Similarly, panels (e) and (f) show the field-dependent absorption behavior for the upper mode. The field was varied between -7 T and +7 T, and the absorption frequency shift was observed as a function of the applied magnetic field.

The absorption spectra reveal that each magnon mode exhibits distinct field-induced absorption depending on the polarization of the incident THz radiation. Specifically, the lower electromagnon (34 cm^{-1}) shows a more prominent activity under RCP, while the upper mode (37 cm^{-1}) exhibits a significant response to LCP. Evaluated chiral polarization reveals a distinct difference between lower and upper

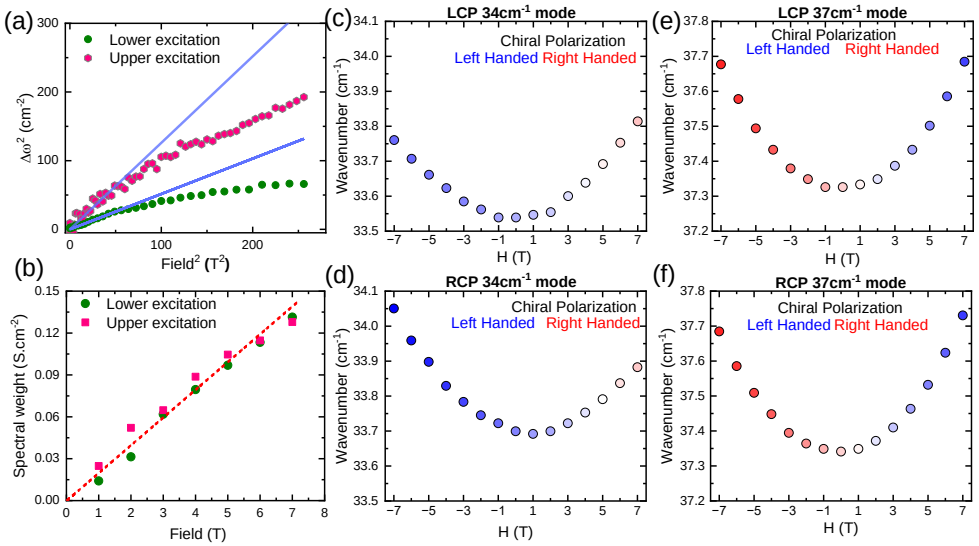

Supplemental Material, Figure S1: **Evolution of magnon central frequency and transmission in the Faraday configuration. a,** Evolution of the magnon mode with magnetic field. The solid line represents a fit using the easy-axis model, as described in the text. **b,** Spectral weight of the imaginary part of the transverse optical Hall conductivity as a function of magnetic field at $T = 4.2$ K. The solid line shows a linear fit to the data. **c–f,** Peak positions of circularly polarized absorption spectra for the lower (34 cm^{-1}) and upper (37 cm^{-1}) magnon modes under left- and right-circularly polarized (LCP/RCP) terahertz radiation. The chiral polarization, defined as $(I_{\mathrm{LCP}} - I_{\mathrm{RCP}})/(I_{\mathrm{LCP}} + I_{\mathrm{RCP}})$, I is the intensity.

electromagnon modes. This asymmetry highlights the chiral nature of the magnon modes and provides direct evidence for the inverse chirality predicted by the modified Kitaev interaction model.

The chiral nature of the magnons can also be seen in the raw data of the Faraday angle rotation measurements. Figure S3 displays color maps of IR transmission in NiI_2 as a function of magnetic field (-7 to 7 T) at 4.2 K in Faraday configuration, for polarizer angles of $+45^0$ (panel a) and -45^0 (panel b) relative to the analyzer. The electromagnon modes near 34 and 37 cm^{-1} exhibit asymmetric field-induced shifts between positive and negative magnetic fields. Therefore, it confirms the effect of chirality on low-frequency excitations, in which polarization-dependent responses differ between opposite fields. We also note that the Faraday angle rotation measurements were performed on a zero-field-cooled sample, whereas the MCD measurements were performed on a field-cooled sample (as in Ref. [3]). However, both methods show the effect of chirality in the electromagnons' spectra. This evidence indicates that domain-induced effects are negligible.

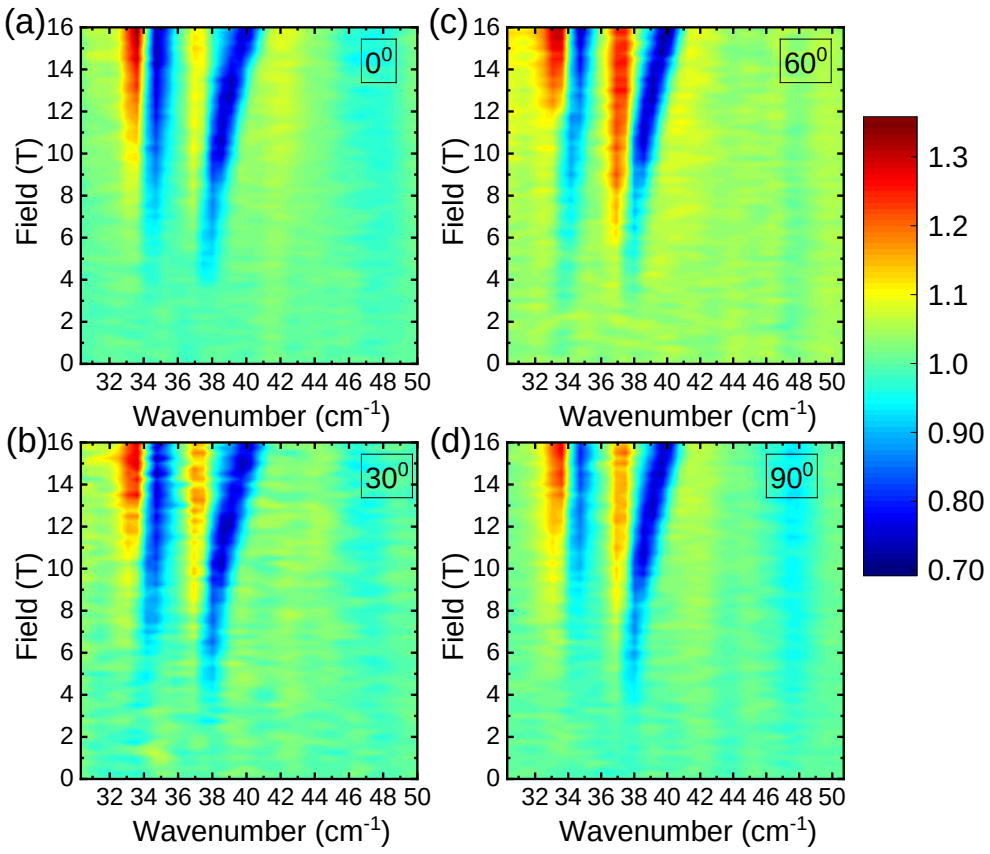

Supplemental Material, Figure S2: **Transmission in the Voigt configuration. a–d,** Magneto-optical response of NiI_2 in the far-infrared spectral range at $T = 4.2$ K in the Voigt geometry ($B \perp E$).

D. Angular dependence of magnon excitations

Figure S2(c-f) shows a 2D color map of the field-dependent transmission spectra $T(B)$, measured in the Voigt configuration for the 4 different a-b plane orientations compared to the applied magnetic field and normalized to the zero-field transmission $T(0)$. Because the background of the transmission spectra shifts with the applied field, we have subtracted the background from each spectrum at each field, keeping the baseline at 1. By comparing the Voigt configuration spectra with those of the Faraday configuration, we see no significant variation in the magnons' central frequency with magnetic field. These findings suggest that the magnon excitation is isotropic in the investigated directions, or that we have not measured the magnons along their respective easy axes. This observation is consistent with the magnetic structure in the multiferroic phase, characterized by a helical modulation with an incommensurate

wave vector $\mathbf{q} \approx (0.138, 0, 1.457)$. The modulation vector forms an angle of approximately 71° with the *ab*-plane, and the spin plane is inclined at about 55° relative to the *c*-axis [4].

E. Emergence of Weak Ferromagnetism and Zero-Field Chirality of Electromagnons

One intriguing feature that LSWT could not explain is the finite chirality of the electromagnons in the absence of an external magnetic field. The presence of chirality at zero field implies spontaneous time-reversal symmetry breaking. In noncollinear magnetic systems, such symmetry breaking is often associated with the emergence of a weak ferromagnetic moment. To examine this possibility, we carefully measured the magnetization and identified a tiny ferromagnetic moment of $10^{-5}\ \mu_B/f.u.$, which has not been reported previously (see Fig. S4). The temperature dependence shows that this weak ferromagnetic moment persists up to 75 K, indicating its close connection to the underlying magnetic order. Moreover, field-dependent magnetization measurements reveal a clear hysteresis loop. Taken together, these observations strongly suggest that the weak ferromagnetic moment originates from a subtle Dzyaloshinskii-Moriya interaction enabled by the multiferroic phase transition. Crucially, this hidden ferromagnetism provides the microscopic origin of the observed zero-field chirality of the electromagnons, directly linking the broken time reversal symmetry to the chiral magnon dynamics.

References

[1] Kittel, C. Theory of Antiferromagnetic Resonance. *Physical Review* **82**, 565–565 (1951). URL http://dx.doi.org/10.1103/PhysRev.82.565.

[2] Keffer, F. & Kittel, C. Theory of Antiferromagnetic Resonance. *Physical Review* **85**, 329–337 (1952). URL http://dx.doi.org/10.1103/PhysRev.85.329.

[3] Kim, J. H. *et al.* Terahertz evidence of electromagnon excitations in the multiferroic van der Waals insulator NiI_2. *Physical Review B* **108**, 064414 (2023). URL http://dx.doi.org/10.1103/PhysRevB.108.064414.

[4] Kuindersma, S., Sanchez, J. & Haas, C. Magnetic and structural investigations on NiI_2 and CoI_2. *Physica B+C* **111**, 231–248 (1981). URL http://dx.doi.org/10.1016/0378-4363(81)90100-5.

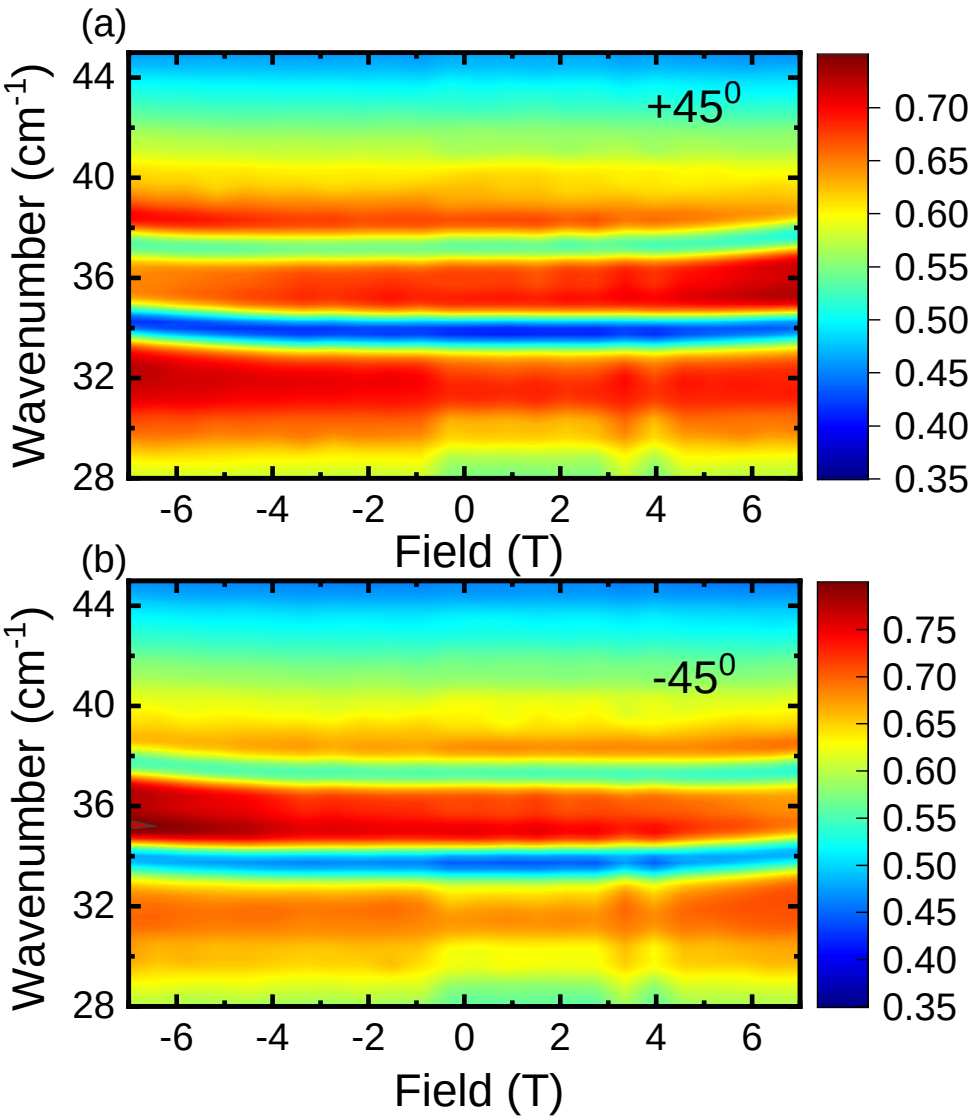

Supplemental Material, Figure S3: **Chiral induced response in IR transmission of NiI_2 a,** Transmission spectra of NiI_2 measured at the $+45^0$ angle of the polarizer with respect to the analyzer at 4.2 K, showing the magnetic field dependence of the 34 and 37 cm^{-1} electromagnon modes. **b,** Corresponding spectra measured at the -45^0 angle of the polarizer with respect to the analyzer at 4.2 K.

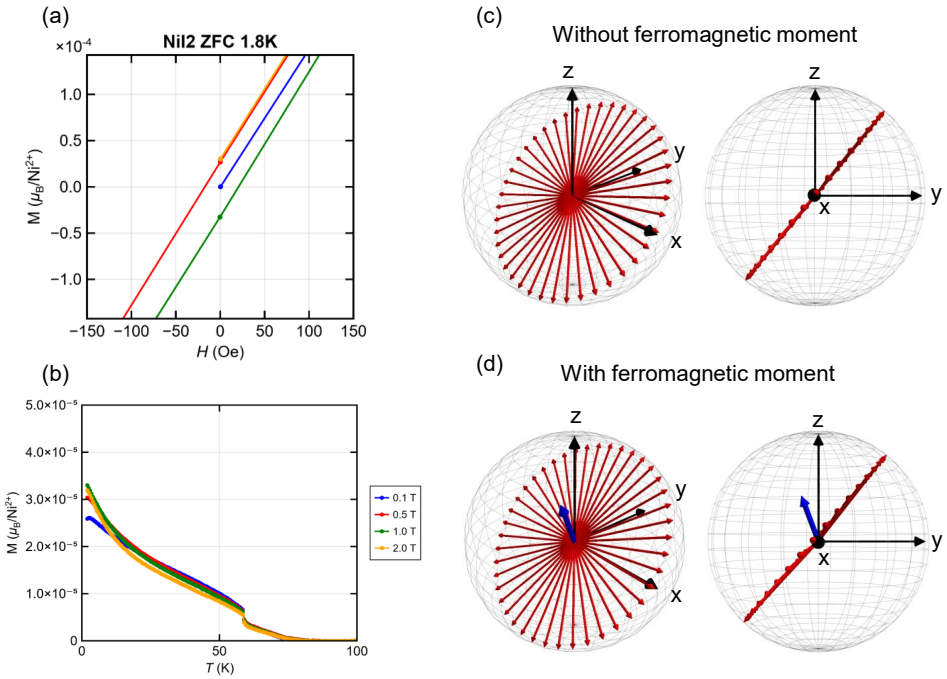

Supplemental Material, Figure S4: **Hidden ferromagnetic moments in NiI_2.** **a,** Field-dependent magnetization measurements of NiI_2 at $T = 1.8$ K with $H \parallel c$. **b,** Temperature dependence of magnetization in NiI_2, measured after field cooling under a finite magnetic field with $H \parallel c$. Each color represents a distinct magnetic field. **c, d,** Bloch sphere representation of the magnetic moments in NiI_2. **c** shows the ideal magnetic structure of NiI_2 without ferromagnetic moments, while **d** depicts the helical magnetic order with weak ferromagnetic moments. The blue arrow indicates the direction of the weak ferromagnetic moments.